Nucleation mechanism and morphology evolution of MoS_2 flakes grown by chemical vapor deposition*

He-Ju Xu(许贺菊)[1,2], Jian-Song Mi(米建松)[1], Yun Li(李云)[1], Bin Zhang(张彬)[1], Ri-Dong Cong(丛日东)[1,†], Guang-Sheng Fu(傅广生)[1,‡], and Wei Yu(于威)[1,¶]

[1] College of Physics Science and Technology, Hebei University, Baoding 071002, China
[2] College of science, North China University of Science and Technology, Tangshan 063009, China

(Received 7 June 2017; revised manuscript received 27 August 2017; published online 20 October 2017)

We study the nucleation mechanism and morphology evolution of MoS_2 flakes grown by chemical vapor deposition (CVD) on SiO_2/Si substrates with using S and MoO_3 powders. The MoS_2 flake is of monolayer with triangular nucleation, which might arise from the initial MoO_{3-x} that is deposited on the substrate, and then bonded with S to form MoS_2 flake. The ratio of Mo and S is higher than 1:2 at the beginning with Mo terminated triangular nucleation formed. After that, the morphology of MoS_2 flake evolves from triangle to similar hexagon, then to truncated triangle which is determined by the faster growth speed of Mo termination than that of S termination under the S rich environment. The nucleation density does not increase linearly with the increase of reactant concentration, which could be explained by the two-dimensional nucleation theory.

Keywords: MoS_2, chemical vapor deposition, morphology, nucleation

PACS: 81.07.Bc, 81.15.Gh, 81.10.–h **DOI:** 10.1088/1674-1056/26/12/128102

1. Introduction

In recent years, two-dimensional materials have gained a great deal of attention from the scientific research and industrial production community as promising materials for the next-generation of ultrathin electronic and optoelectronic devices.[1–3] Graphene, as the most famous member of two-dimensional materials, possesses extraordinary properties and is readily integrated in various applications.[4,5] Compared with graphene, which is a semi-metal with no band gap by nature, transition metal dichalcogenide (TMD) with a substantial band gap has been investigated extensively. As a typical TMD material, MoS_2 has been found to have electronic applications because of its unique and exciting properties, such as the thickness-dependent band gap transition: from a direct band gap of 1.9 eV for a monolayer to an indirect one of 1.3 eV for bulk,[6–8] excellent carrier mobility with a high on-off ratio,[9,10] and valley-related physics.[11,12] These attract a large number of researchers who dedicate themselves to exploring its unique performance and application research of the device from electronics to battery materials. Nevertheless, large-scale, layer-controlled and high-quality two-dimensional MoS_2 should be prepared for meeting its various application demands.

There are generally two kinds of preparation methods for two-dimensional MoS_2, including top-down methods, such as mechanical exfoliation,[9] chemical exfoliation,[13] and direct sonication in solvents,[14] which separate the stacked thick layers (or even bulk materials) of MoS_2. However, the resulting MoS_2 are typically microscale with poor thickness uniformity, ranging from monolayer to tens of layers. To improve this, several bottom-up methods have been developed to directly synthesize large-area MoS_2 monolayers onto SiO_2/Si substrates, such as the sulphurisation of pre-deposited Mo[15] or Mo oxide[16] layers, the decomposition of thiomolybdates,[17] and chemical vapor deposition (CVD) through a gas-phase reaction of MoO_3 and S.[18] Among these, CVD is the most promising method to obtain high-quality MoS_2 films. The CVD-grown films usually have a variety of shapes, such as triangle, similar hexagon, truncated triangle, dendritic and polygonal shapes.[19] The growths of different shapes would result in different crystal grain boundaries, and then affect the boundary energy in growth dynamics, even the quality of film. Thus, the nucleation mechanism and morphology evolution research would be the critical factors for fabricating the large area and high-quality MoS_2.

In this work, we report the directly CVD synthesis of MoS_2 flakes by using solid S and MoO_3 powders on sloping SiO_2/Si substrates. The nucleation mechanism and morphol-

*Project supported by the National Natural Science Foundation of China for Youths (Grant No. 61504036), the Natural Science Foundation of Hebei Province for Youths, China (Grant No. A2016201087), the Doctoral Fund of the Ministry of Education of China (Grant No. 20131301120003), and the Science and Technology Project of Hebei Province, China (Grant No. 13214315).

†Corresponding author. E-mail: congrd@hbu.edu.cn
‡Corresponding author. E-mail: fugs@hbu.cn
¶Corresponding author. E-mail: yuwei@hbu.edu.cn

© 2017 Chinese Physical Society and IOP Publishing Ltd

ogy evolution of MoS_2 grown by CVD are investigated. The results point out that the original nucleus is triangle. With the growth progress, the final shape of MoS_2 flakes could be determined by the growth speed of Mo termination and S termination sides under the S rich environment. The nucleation density also could be controlled by controlling the reactant concentration.

2. Experiment

MoS_2 flakes were fabricated in a double heating zone furnace with a 50-mm-diameter quartz tube as shown in Fig. 1(a). A ceramic boat containing 200-mg sulfur powder (99.999%, Sigma-Aldrich) was placed in the first heating zone of the furnace, 10-mg MoO_3 powder (99.99%, Sigma-Aldrich) was placed in the second heating zone of the furnace, and 300-nm-thick SiO_2/Si substrate was placed slopingly downstream 6 cm away from the MoO_3 powder. The furnace was first evacuated to lower than 2 Pa using a vacuum pump and then purged 3 times with Ar. The MoO_3 powder was heated to 900 °C with a heating rate of 15 °C/min. In the fabricating process, the S and MoO_3 were set to achieve the highest temperature at the same time. Therefore, S started to heat to 190 °C with the heating rate of 20 °C/min when MoO_3 is 760 °C, and then maintained for 20 min with 130 sccm of Ar followed by natural cooling. The working pressure is 200 Pa.

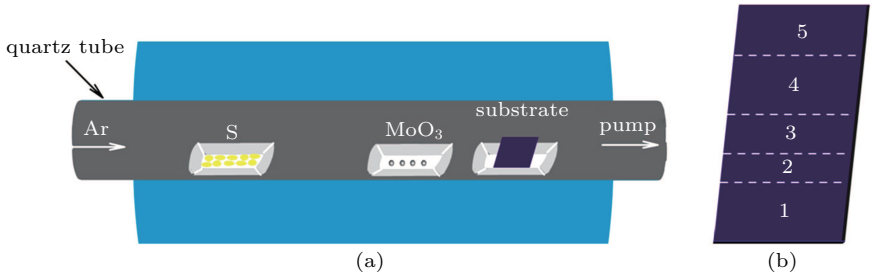


Fig. 1. (color online) Schematic illustrations of (a) growth set up and (b) substrate sectioned into 5 parts.

3. Characterization

The MoS_2 flakes were characterized by scanning electron microscopy (SEM) using the Nova NanoSEM 450 instrument, atomic force microscopy (AFM) recorded using a tapping mode in a Bruker Multimode 8 AFM system, and Raman spectroscopy and photoluminescence conducted using a JY Horiba Labram HR800 Evolution imaging confocal Raman microscope under an excitation wavelength of 532 nm.

4. Results

Figure 1(b) shows the schematic illustration of the SiO_2/Si substrate sectioned into five parts according to the different reactant concentrations along the direction vertical to the gas flow. The corresponding SEM images of the five sections are shown in Fig. 2, which exhibits the evolution of MoS_2 flakes. There are no triangular MoS_2 flakes in section 1 at the bottom of the substrate as shown in Fig. 2(a), since the reactant concentration is too low for the further growing of the MoS_2 flakes. In section 2 as shown in Fig. 2(b), MoS_2 flakes with triangular shape[20] randomly distributed on the substrate and with an average size of about 2 μm (inset of Fig. 2(b)), indicating that more reactants reach here and incorporate into the MoS_2 flakes. The triangular flake further develops into a similar hexagon in Fig. 2(c) (section 3) with the distance of the two opposite sides being about 2.5 μm (inset of Fig. 2(c)). In this section, the growth rates of crystal faces of S and Mo termination are close to conformity, indicating that the preferential growth of the crystal face is inhibited, which leads to the similar hexagon MoS_2 flakes. The nucleation density of section 3 does not change obviously compared with the scenario in section 2: it has only a little bit of increase in size and the morphology changes from triangular to a similar hexagon. In section 4 as shown in Figs. 2(d) and 2(e), a similar hexagon is converted into a truncated triangle with the size increasing from 4 μm to 14 μm, and a crystal face preferential growth mode appears again. In this section, the nucleation density increases with the increase of the reactant concentration. Meanwhile, some new triangles begin to grow on the same nucleation site at the center of the truncated triangles, which are all distributed randomly.[21] The growth of a new layer occurs also at some non-nucleation points since there might be some defects. With the further increase of the reactant concentration, adjacent MoS_2 flakes connected to each other with few overlaps at the border (the color change does not appear obviously at the border in Fig. 2(f) (section 5)). The two-dimensional grain boundaries meet, merge and disappear, and even connect to a layer, which can be explained by the theory of multi two-dimensional nucleation growth discussed in the following part.

The AFM, Raman and PL spectra are used to evaluate the thickness and quality of the MoS_2 flakes. The height image obtained from a tapping mode AFM measurement is shown in Fig. 3(a). The height profile drawn at the edge as shown in Fig. 3(b) reveals a film thickness of ~ 0.7 nm, which agrees well with one atomic layer of MoS_2 flakes.[22]

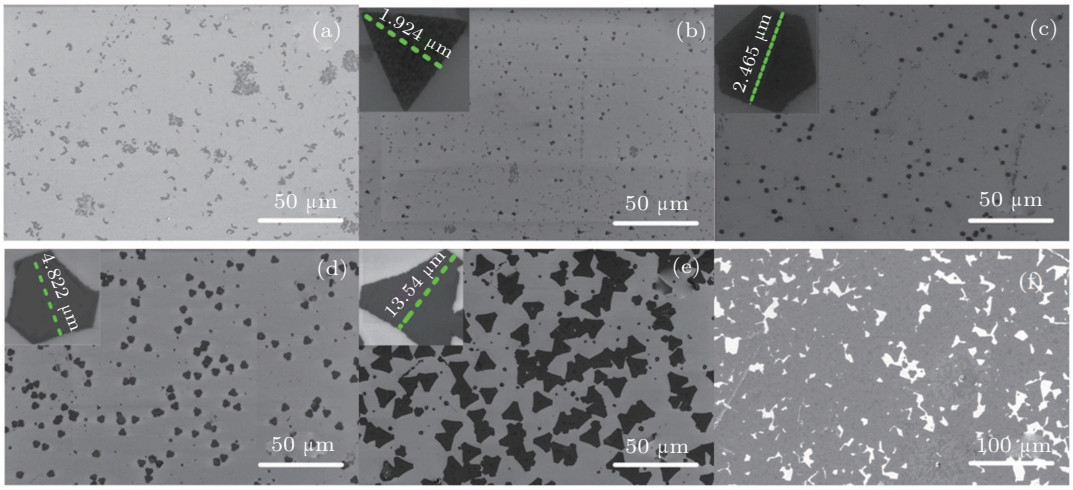


Fig. 2. (color online) SEM images in five sections: panels (a), (b), (c), and (f) for sections of 1, 2, 3, and 5; panels (d) and (e) for section 4 from down to up.

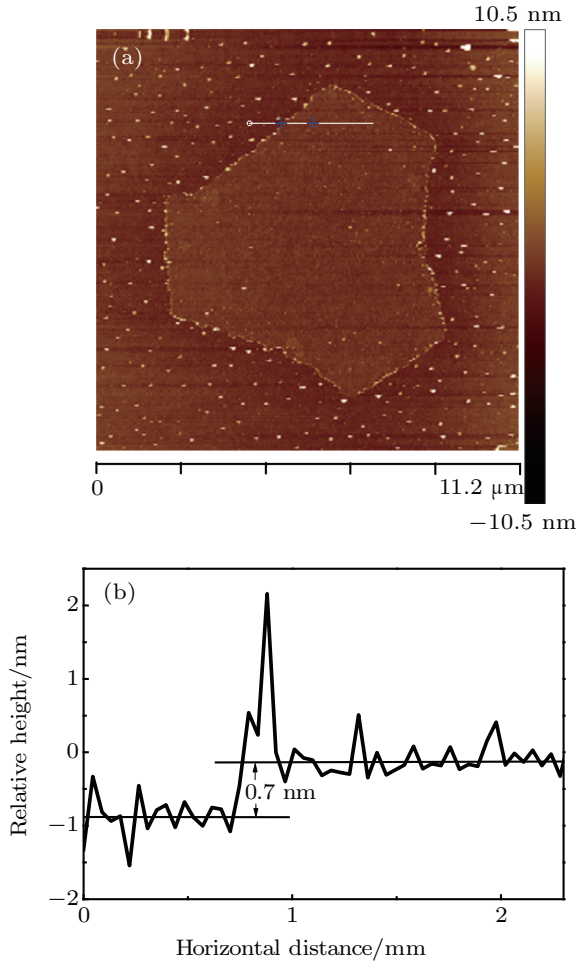


Fig. 3. (color online) (a) AFM images of a MoS_2 flakes on SiO_2/Si substrate and (b) profile along the line in panel (a).

Figure 4(a) shows the spectra of MoS_2 flakes with different morphology and different regions marked as curves 1-5 (insets of Fig. 4(a)). Raman peaks corresponding to in-plane vibrations of Mo and S atoms (E^1_{2g} mode) and out-of-plane vibration of the S atom (A_{1g} mode)[23] are exhibited in curves 1–4 respectively, but do not emerge in curve 5, which indicates that the outside of the triangle is the substrate without the MoS_2 flakes. The differences between the two peaks (Δk) from curves 1–4 gradually increase. The $\Delta k \sim 20.4$ cm^{-1} of the small triangle (region 1) is close to synthesized monolayer MoS_2,[8] but larger than that of exfoliated monolayer MoS_2 ($\Delta k < 20$ cm^{-1}),[24] which is likely to be attributed to the defects that are introduced in the synthesis process. The increases of Δk in curves 2 and 3 regions might be caused by more defects introduced in the growing process, however, the

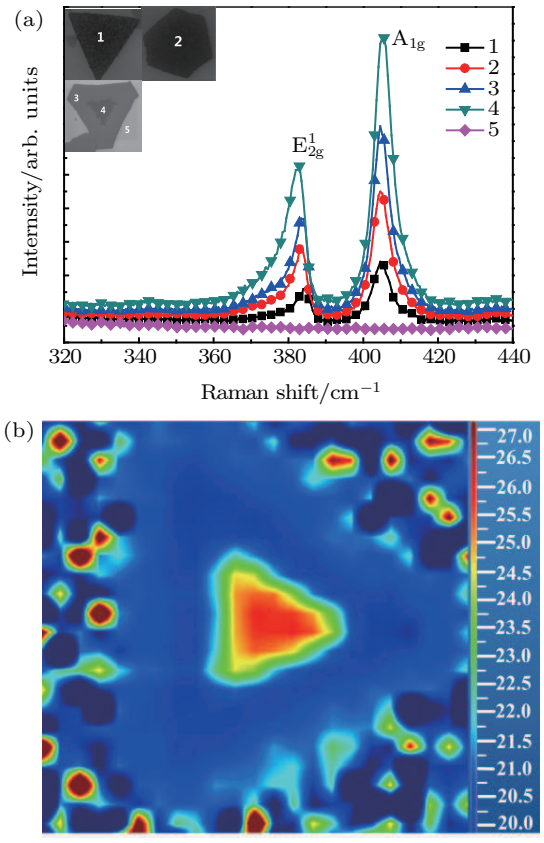


Fig. 4. (color online) (a) Raman spectra of different regions marked as 1–5 in the inset, the inset shows SEM images of the small triangle, the similar hexagon, the edge of truncated triangle, the center of truncated triangle and the outside of the triangle marked as 1–5 correspondingly, (b) Raman mapping of the magnitude of the frequency difference between A_{1g} and E^1_{2g}.

Δk of region 4 increases to 23.2 cm^{-1}, which is corresponding to multilayer MoS_2. Besides, the full width at half-maximum (FWHM) of the E^1_{2g} peak in region 1 is ~ 4.5 cm^{-1},[25] which further confirms the monolayer nature and high quality of the MoS_2 flakes. Figure 4(b) shows the Raman mapping of a truncated triangle with a new small triangle in the center by plotting the 2D spatial variation of the magnitude of the frequency difference between the A_{1g} and E^1_{2g} peaks to show the thickness uniformity. At the edge of the truncated triangle, most of the flakes have a Δk of < 21 cm^{-1}, confirming a homogeneous monolayer. An obvious increase in the frequency difference can be observed in the center of the triangular domain, which indicates that some new layers grow on the original MoS_2 flakes. This confirms the SEM results in Fig. 2(e).

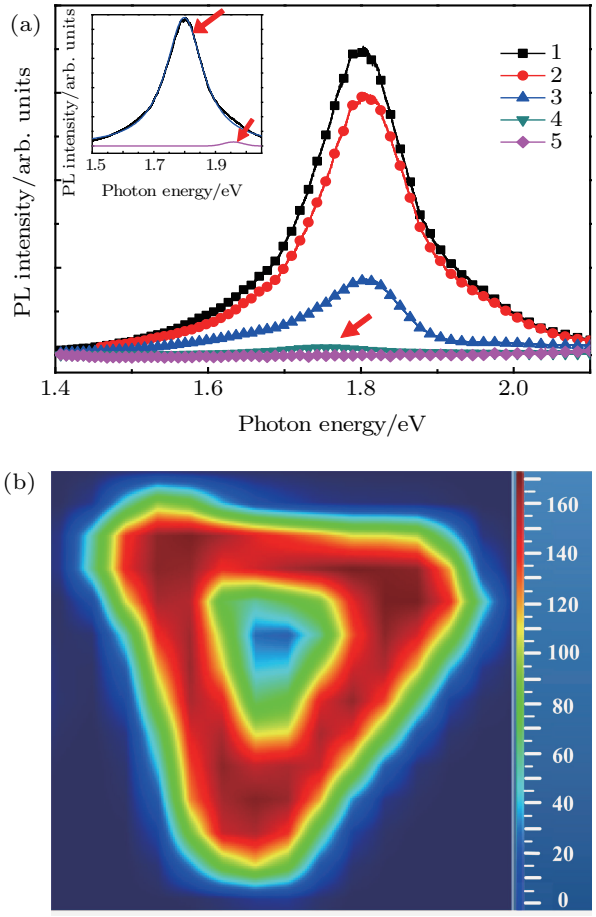


Fig. 5. (color online) (a) PL spectra of different areas marked as 1–5 in the inset of figure 4(a), (b) mapping image of the PL intensity of the truncated triangle.

Figure 5(a) shows the typical PL spectra of different regions marked as 1–5 in the insert of Fig. 4(a). The PL spectra are normalized by the Raman peak intensity to exclude external environmental effects such as laser power and local electric field factors. Pronounced luminescence emissions in 1–3 regions are observed at about 1.80 eV as well as a shoulder that can be seen at 1.96 eV as shown in the inset of Fig. 5(a), which can be correlated to the A and B exciton transition arising from the direct gap transition at the K point for the monolayer MoS_2.[26] The PL intensities of 1–3 regions gradually decrease, which could be attributed to a large number of defects in the synthesis process. In contrast to the strong PL of monolayer MoS_2 flakes (region 1–3), the center of the truncated triangle with new layers (region 4) exhibits a weak peak at 1.75 eV, which corresponds to an indirect transition at lower energy. This distinguishing PL behavior of the multilayer MoS_2 flakes indicates that luminescence quantum efficiency is much higher in MoS_2 monolayer than in multilayer.[27] This could also be observed in PL mapping in Fig. 5(b), in which the monolayer region is uniform and exhibits much stronger emission than the multilayer region.

5. Discussion

The morphologies of the MoS_2 flakes evolve from triangle, similar hexagon to truncated triangle from sections 1 to 5 and the size of MoS_2 flakes increase gradually with the increase of the reactant concentration. In the growing process, the triangle MoS_2 nucleates first under any reactant concentration.[19] This could be explained as the fact that the volatile MoO_{3-x} species are initially deposited from the reduced MoO_3 by the sulfur vapor, and then MoO_{3-x} species further react with sulfur vapor to form MoS_2 flakes,[28] which leads to the ratio of Mo and S more than 1:2 at the beginning of the growing process. Therefore, the triangular Mo terminated nucleation is formed.[18] The morphologies of MoS_2 flakes further evolve when the sizes of the triangles each reach 2 μm as shown in Fig. 2(c). The triangle evolves to a similar hexagon and then to a truncated triangle with the increase of the size. In this stage, the growth of MoS_2 is under the S rich environment, the Mo termination grows faster than S termination, leading to the change of the sides from Mo termination to S termination. Meanwhile, the MoS_2 morphology evolves from a Mo termination triangle to a similar hexagon with three sides of Mo termination and the other three equal sides of S termination, and then to truncated triangles with three long sides of S termination and three short sides of Mo termination as shown in Fig. 6.

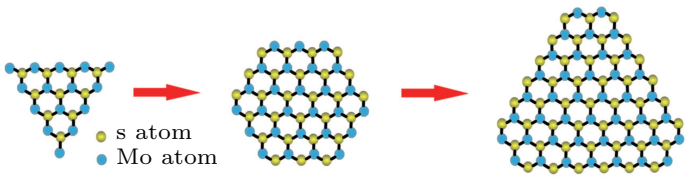


Fig. 6. (color online) Schematic illustration of morphologies of MoS_2 flakes in growth process.

In conclusion, we find that the nucleation of monolayer MoS_2 flake is a triangle. The final shape of MoS_2 flake is determined by the faster growth speed of Mo termination than that of S termination under the S rich environment.

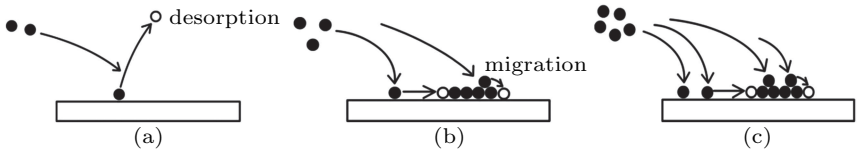


Fig. 7. Schematic illustrations of the typical growth processes during the CVD growth of MoS_2 films.

The nucleation density does not increase linearly with the increase of the reactant concentration in the growth process of the MoS_2 flakes, which is corresponding to the two-dimensional nucleation theory. The nucleation mechanism can be explained as follows: in the process of Gas-solid phase transition,

$$\Delta G = RT \ln P_0/P,$$

where ΔG is the variation of free energy, R is the universal gas constant, T is the thermodynamic temperature, P is the supersaturated vapor pressure, and P_0 is the equilibrium vapor pressure. In order to make the phase transition occur spontaneously, that is, $\Delta G < 0$, the P should be greater than P_0. Therefore, the supersaturated vapor pressure is the driving force for the phase transformation process. In section 1, the reactant concentration is low for MoS_2 to nucleate ($P < P_0$), so there are no nuclei formed as shown in Fig. 7(a). In section 2, the reactant concentration is higher ($P > P_0$) and steady nuclei are randomly distributed at the defect sites of the substrate. The growth can be understood from a thermodynamics view as shown in Fig. 7(b). The interface and surface free energy of nucleation in defects are lower than the surface free energy of the substrate, inducing MoS_2 species to only need to diffuse a comparatively short distance to coalesce into the nuclei already formed rather than initiating new ones,[29] and then develops into MoS_2 flake. In this process, nucleation density remains nearly unchanged and only the size of MoS_2 flake increases with the increase of the reactant concentration. In section 4, the supersaturated vapor pressure is higher, and MoS_2 species form new nuclei at the defects and the original nucleation points before they can diffuse to the nuclei edge to form MoS_2 flakes as shown in Fig. 7(c). Therefore, the nucleation concentration increases and multilayer growth on original monolayer MoS_2 flakes emerges.

6. Conclusions

In this work, triangle, similar hexagon and truncated triangle MoS_2 flakes are synthesized on SiO_2/Si substrates by chemical vapor deposition. Our results reveal that the original nuclei are triangle in shape. The final shape and size of MoS_2 flake are determined by the faster growth speed of Mo termination than that of S termination under S rich environment. The nucleation density does not increase with the reactant concentration increasing linearly. Through reasonably controlling the nucleation density, crystal size and shape, high-quality monolayer MoS_2 flakes could be obtained. Our results are expected to be useful in further studying the MoS_2 growth and the scaled layer-controlled high-quality MoS_2 flakes for a wide range of applications.

References

[1] Schwierz F 2010 *Nat. Nanotechnol.* **5** 487
[2] Wang R, Chien H C, Kumar J, Kumar N, Chiu H Y and Zhao H 2014 *ACS Appl. Mater. Inter.* **6** 314
[3] Wang Q H, Kalantar-Zadeh K, Kis A, Coleman J N and Strano M S 2012 *Nat. Nanotechnol.* **7** 699
[4] Lancellotti L, Polichetti T, Ricciardella F, Tari O, Gnanapragasam S, Daliento S and Di Francia G 2012 *Thin Solid Films* **522** 390
[5] Yin Z, Zhu J, He Q, Cao X, Tan C, Chen H, Yan Q and Zhang H 2014 *Adv. Energy Mater.* **4** 1
[6] Ganatra R and Zhang Q 2014 *ACS Nano.* **8** 4074
[7] Padilha J E, Peelaers H, Janotti A and Van de Walle C G 2014 *Phys. Rev. B* **90** 205420
[8] Park J W, So H S, Kim S, Choi S H, Lee H, Lee J, Lee C and Kim Y 2014 *J. Appl. Phys.* **116** 183509
[9] Radisavljevic B, Radenovic A, Brivio J, Giacometti V and Kis A 2011 *Nat. Nano.* **6** 147
[10] Lin M W, Liu L, Lan Q, Tan X, Dhindsa K, Zeng P, Naik V M, Cheng M M and Zhou Z 2012 *J. Phys. D: Appl. Phys.* **45** 345102
[11] Zeng H, Dai J, Yao W, Xiao D and Cui X 2012 *Nat. Nanotechnol.* **7** 490
[12] Mak K F, He K, Shan J and Heinz T F 2012 *Nat. Nanotechnol.* **7** 494
[13] Eda G, Yamaguchi H, Voiry D, Fujita T, Chen M and Chhowalla M 2011 *Nano Lett.* **11** 5111
[14] Coleman J N, Lotya M and O'Neill A 2011 *Science* **331** 568
[15] Laskar M R, Ma L, Kannappan S, Sung Park P, Krishnamoorthy S, Nath D N, Lu W, Wu Y and Rajan S 2013 *Appl. Phys. Lett.* **102** 252108
[16] Mann J, Sun D, Ma Q, Chen J R, Preciado E, Ohta T, Diaconescu B, Yamaguchi K, Tran T, Wurch M, Magnone K, Heinz T F, Kellogg G L, Kawakami R and Bartels L 2013 *Eur. Phys. J. B* **86** 226
[17] Lin Y C, Zhang W, Huang J K, Liu K K, Lee Y H, Liang C T, Chu C W and Li L J 2012 *Nanoscale* **4** 6637
[18] Wang S, Rong Y, Fan Y, Pacios M, Bhaskaran H, He K and Warner J H 2014 *Chem. Mater.* **26** 6371
[19] Ji Q, Zhang Y, Zhang Y and Liu Z 2015 *Chem Soc Rev.* **44** 2587
[20] van der Zannde A M, Huang P Y, chenet D A, Berkelbach T C, You Y, Lee G H, Heinz T F, Reichman D R, Muller D A and Hone J C 2013 *Nat. Mater.* **12** 554
[21] Shaw J C, Zhou H, Chen Y, Weiss N O, Liu Y, Huang Y and Duan X 2014 *Nano Res.* **7** 511
[22] Tao J, Chai J, Lu X, Wong L M, Wong T I, Pan J, Xiong Q, Chia D and Wang S 2015 *Nanoscale* **7** 2497
[23] Korn T, Heydrich S, Hirmer M, Schmutzler J and Schüller C 2011 *Appl. Phys. Lett.* **99** 102109
[24] Sundaram R S, Engel M, Lombardo A, Krupke R, Ferrari A C, Avouris Ph and Steiner M 2013 *Nano Lett.* **13** 1416
[25] Liu H, Ansah Antwi K K, Ying J, Chua S and Chi D 2014 *Nanotechnology* **25** 405702
[26] Mouri S, Miyauchi Y and Matsuda K 2013 *Nano Lett.* **13** 5944
[27] Splendiani A, Sun L, Zhang Y B, Li T S, Kim J H, Chim C Y, Galli G and Wang F 2010 *Nano Lett.* **10** 1271
[28] Liang T, Xie S, Huang Z T, Fu W F, Cai Y, Yang X, Chen H Z, Ma X Y, Iwai H, Fujita D, Hanagata N and Xu M S 2016 *Adv. Mater. Interfaces* 1600687
[29] Zhang J, Yu H, Chen W, Tian X, Liu D, Cheng M, Xie G, Yang W, Yang R, Bai X, Shi D and Zhang G 2014 *ACS Nano* **8** 6024